Supporting Information for

Noble Metal-free Ternary Cobalt-Nickel Phosphides for Enhanced Photocatalytic Dye-Sensitized Hydrogen Evolution and Catalytic Mechanism Investigation

Zhixing Cheng†§, Yiqin Xu†, and Bin Fei*§

E-mail: zhixing.cheng@polyu.edu.hk, bin.fei@polyu.edu.hk

† Institute of Semiconductors, Guangdong Academy of Sciences, Guangzhou 510070, P.R. China

§ School of Fashion & Textiles, The Hong Kong Polytechnic University, Hong Kong 100872, P.R. China

Table of Contents

Supplementary illustrations and explanations

I. Experimental Procedures

1. Electrochemical measurements

The electrochemical tests are conducted on an electrochemical workstation (CHI760E, CH instrument) with a conventional three-electrode cell. A Pt plate (1cm × 1cm) is employed as the counter electrode and an Ag/AgCl (saturated KCl) electrode was used as the reference electrode. The working electrode is prepared on a glassy carbon electrode (GCE) with a diameter of 5 mm. The exposed area of the working electrode is 0.19625 cm^2. The GCE is polished with α–Al_2O_3 powder with decreasing sizes (1.0-0.05 μm), and it is then ultrasonically washed with deionized water and absolute ethanol before the samples were coated on it.

The electrode materials are prepared by dispersing 5 mg of the catalyst and 1 mL mixed solution, which is compounded by 25 μL of Nafion solution, 250 μL of ethanol and 750 μL of water. The mixture was then sonicated for about 1 h at room temperature to form a homogeneous ink. 10 μL of the ink (containing 0.05 mg of catalyst) was loaded onto the GCE, giving a loading mass of 0.25 mg cm^{-2}. The same procedure was used for all of the samples during their electrode preparation. The photocurrent measurements were carried out with the electrolyte and 1 M aqueous KOH (pH = 14). The electrochemical impedance spectroscopy (EIS) and cyclic voltammetry measurements are respectively performed in the solution by applying an AC voltage with -1.5 mV amplitude in a frequency range from 1 Hz to 100 kHz. The bias sweep range is from 0 to -0.9 V; the scanning rate of 0.1 V/s. The polarization curve is performed in the same solution with the bias sweep range from -1.4 to -1.8 V vs Ag/AgCl.

2. Computational methodology

The first-principles calculations are performed in the framework of the density functional theory with the projector augmented plane-wave method, as implemented in the Vienna ab initio simulation package.[1] The generalzied gradient approximation proposed by Perdew, Burke, and Ernzerhof is employed for the exchange-correlation

potential.[2] The long range van der Waals interaction is described by the DFT-D3 approach.[3] The spin-polarized are considered in the calculations. The Ni_2P (111) surface containing 48 Ni atoms and 24 P atoms, the top two layers of Ni and P atoms are allowed to relax, while the bottom two layers of Ni and P atoms are fixed. The CoNiP (111) surface containing 24 Co atoms, 24 Ni atoms, and 24 P atoms, the top two layers of Co, Ni and P atoms are allowed to relax, while the bottom two layers of Co, Ni and P atoms are fixed. The vacuum layers of 15 Å are added perpendicular to the slabs to avoid artificial interaction between periodic images. The cut-off energy for plane wave is set to 450 eV. The Brillouin zone integration is performed using a 1×1×1 k-mesh for the structural optimization, while a dense k-point mesh of 3×3×1 was used to calculate the density of states. The converged conditions for electronic and ionic optimizations are respectively chosen as 1×10^{-5} eV and 0.02 eV/Å.

II. Supplementary illustrations and explanations

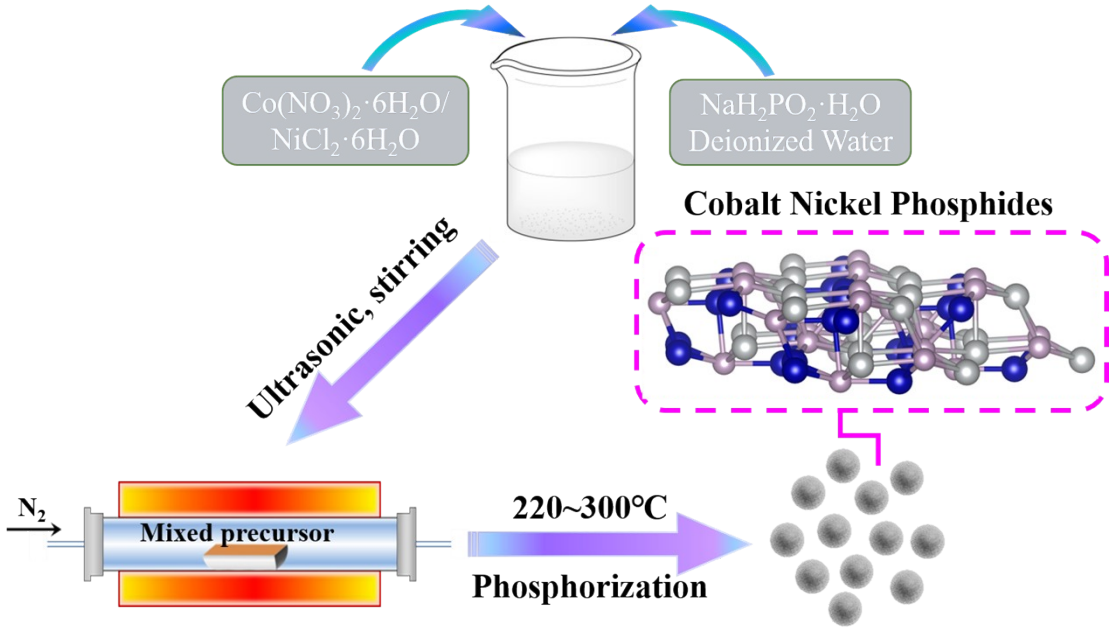

Scheme S1. The preparation process of phosphides: the synthesis of precursors using a mixture of Co and Ni salts and NaH_2PO_2 solution, followed by phosphide formation through annealing under an inert atmosphere.

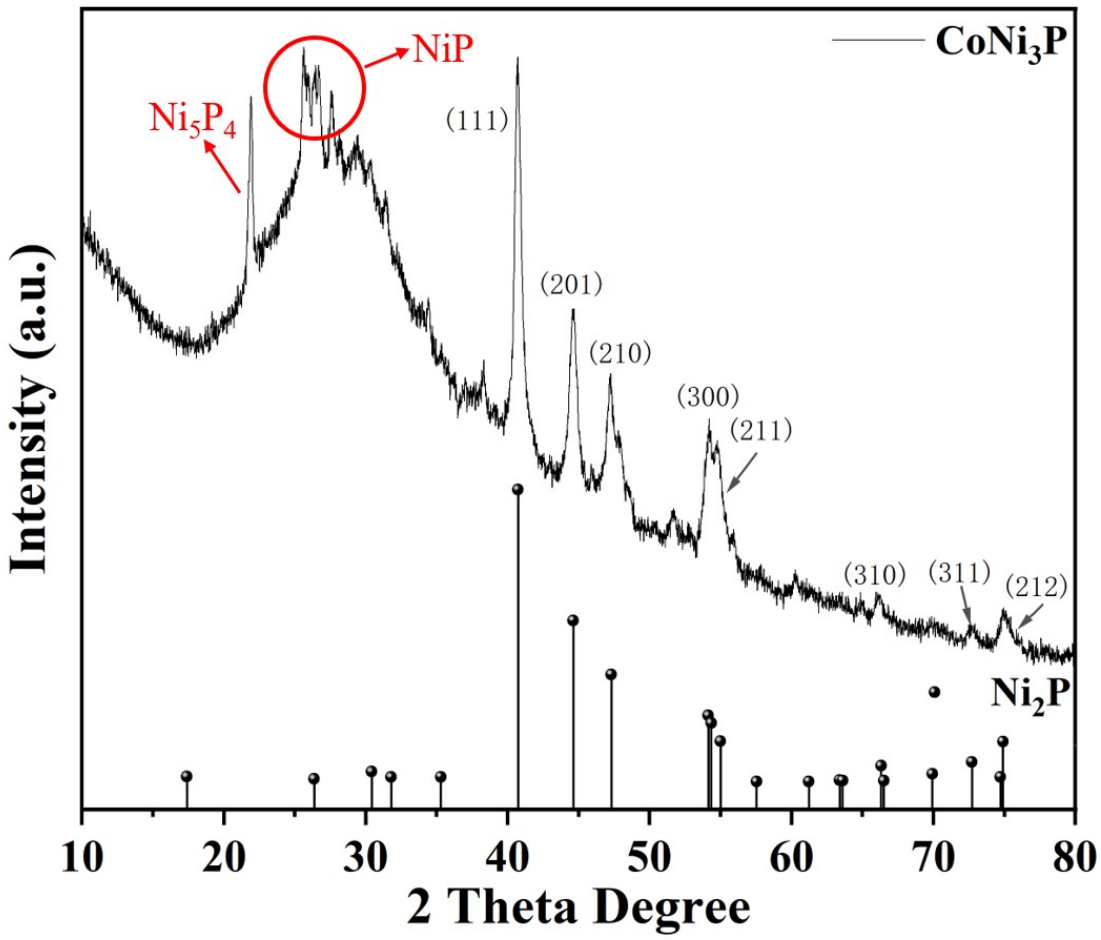

Figure S1. Powder XRD pattern of as-prepared $CoNi_3P$. The mixed phases may contain NiP and Ni_5P_4.

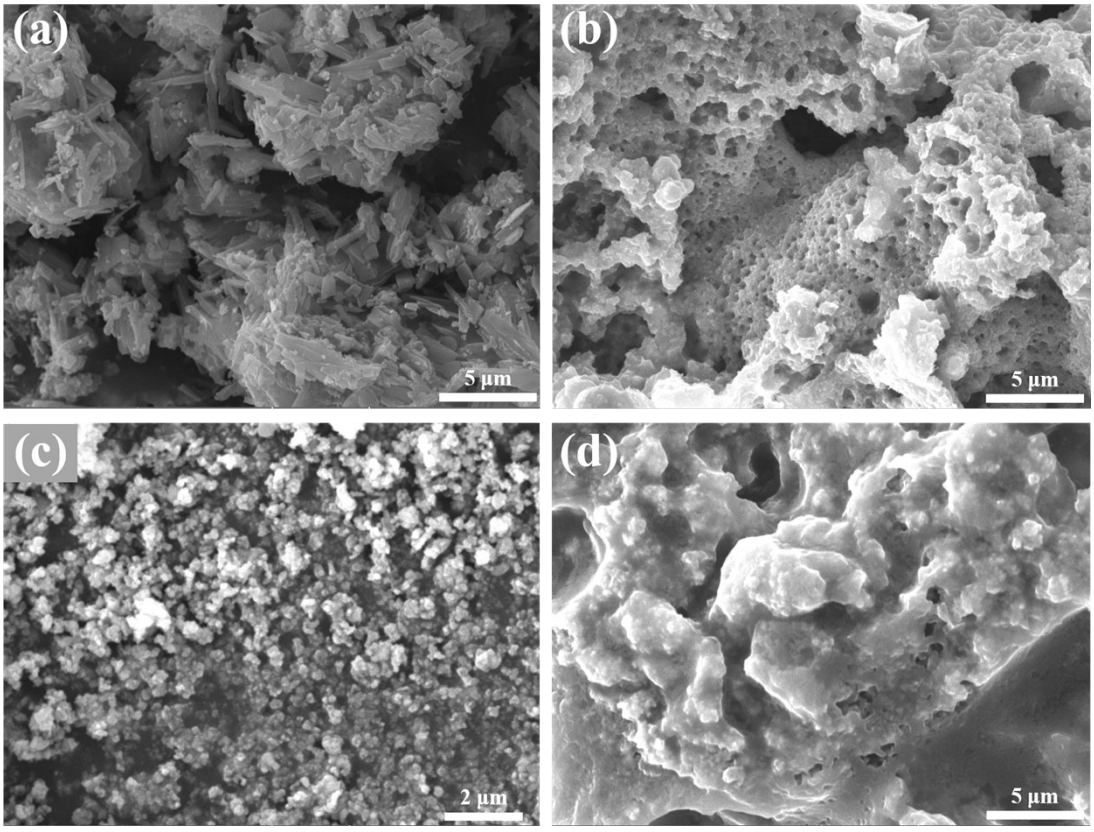

Figure S2. The SEM images of the **(a)** CoP, **(b)** CoNiP, **(c)** Ni_2P and **(d)** $CoNi_3P$ samples.

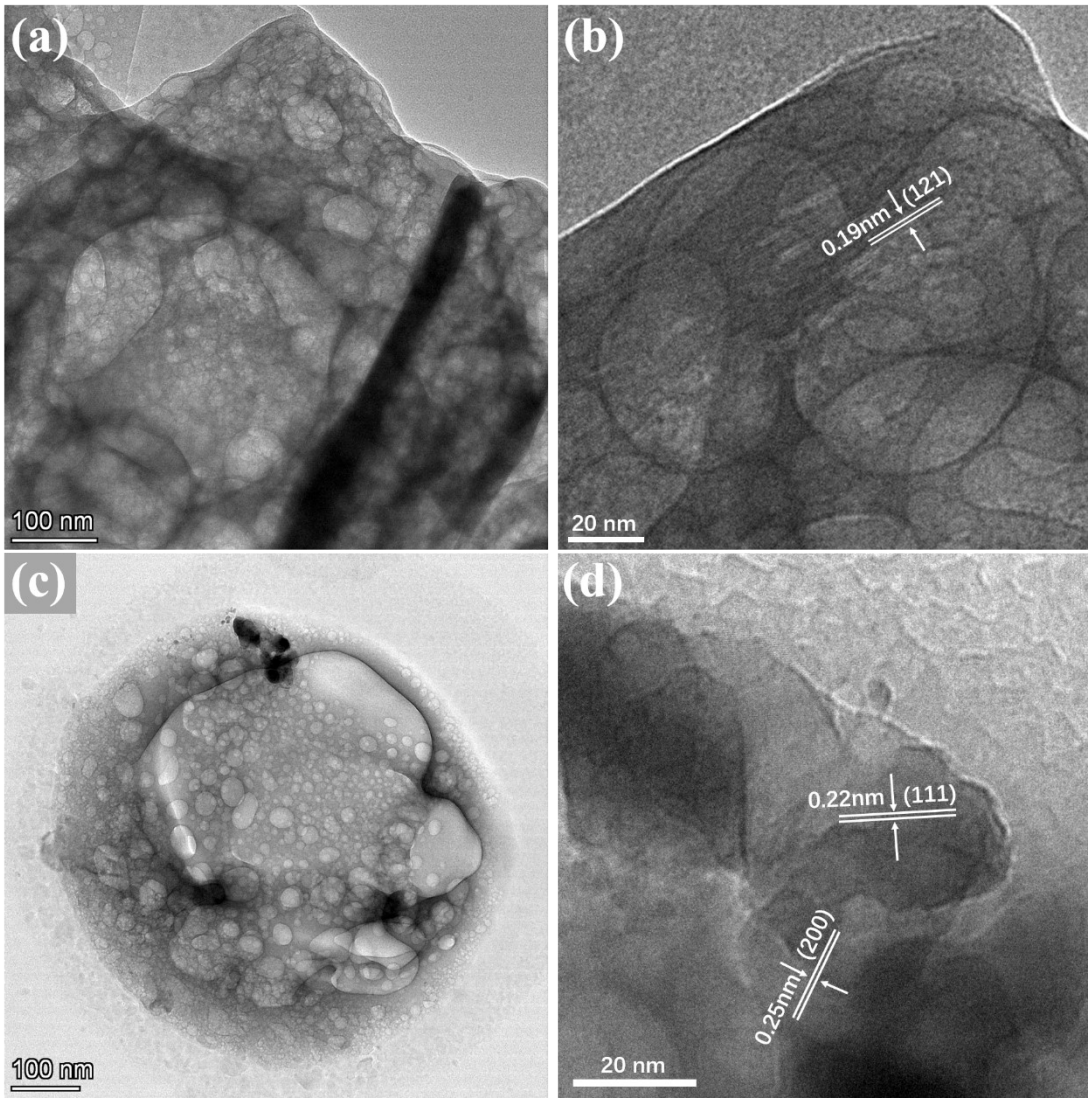

Figure S3. The TEM and HRTEM images of **(a, b)** the CoP and **(c, d)** the $CoNi_3P$ samples.

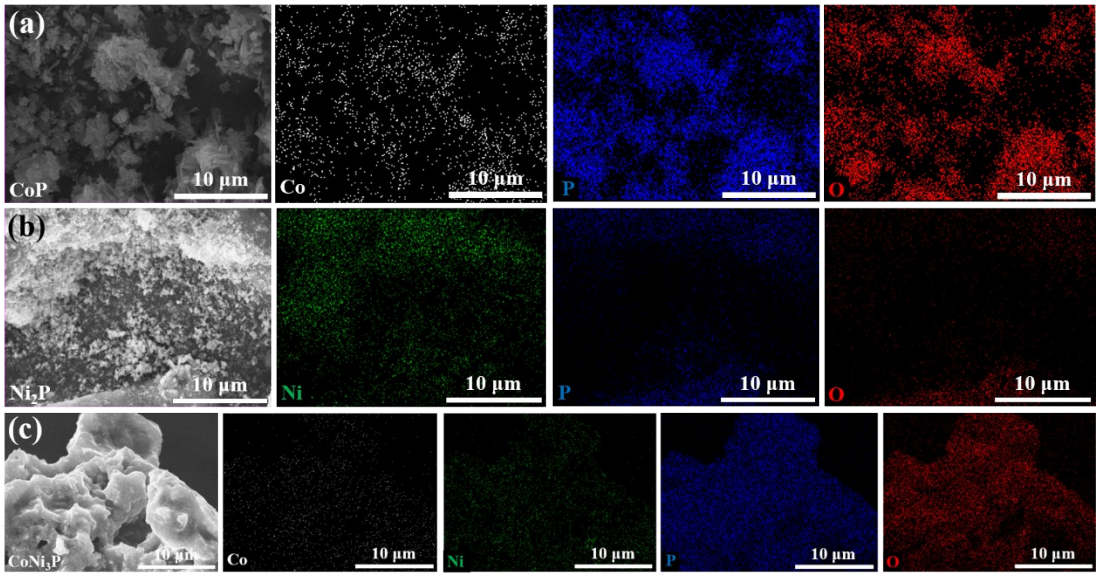

Figure S4. The elemental mapping images of **(a)** CoP, **(b)** Ni_2P and **(c)** $CoNi_3P$ samples.

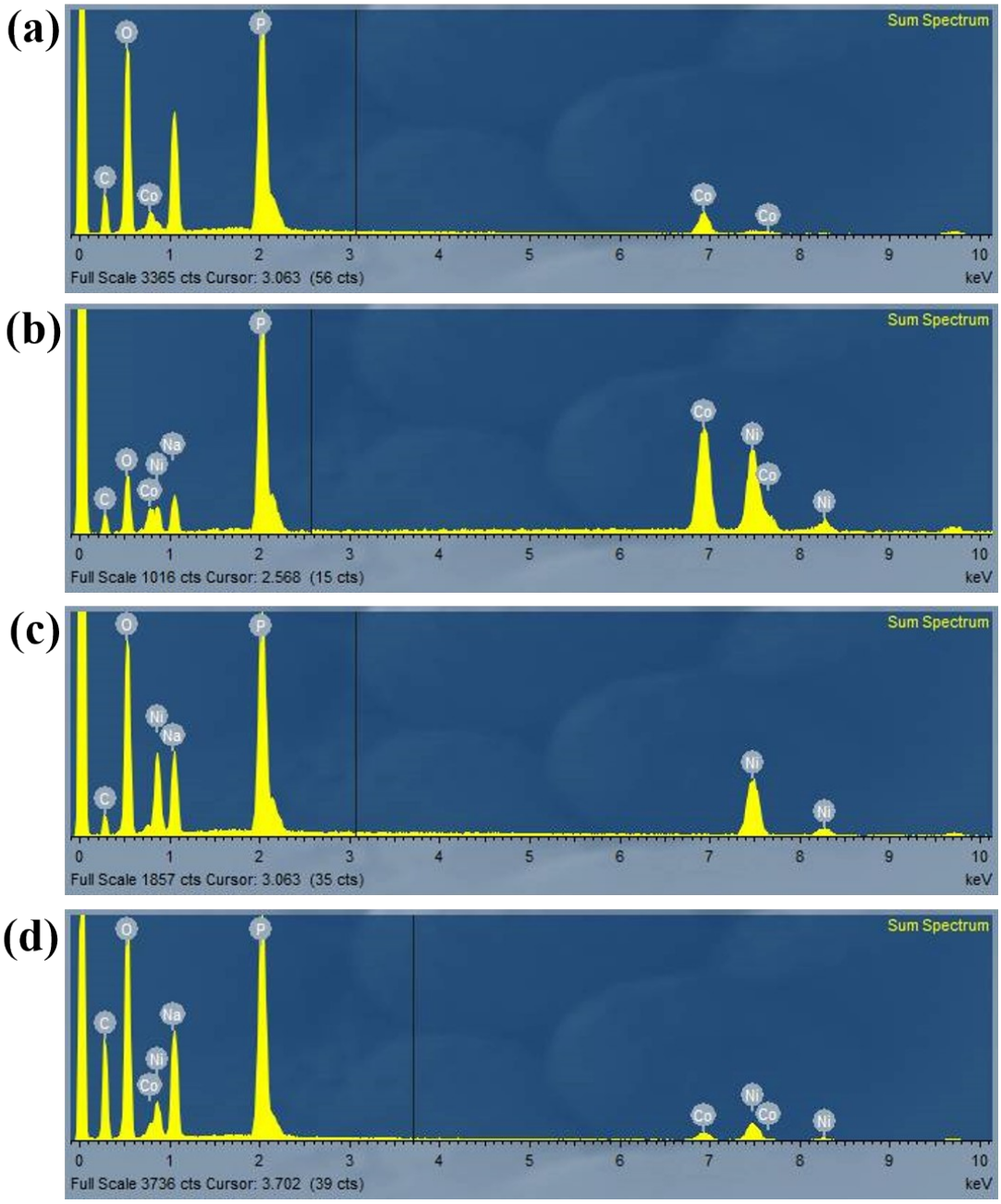

Figure S5. The EDX patterns of **(a)** CoP, **(b)** CoNiP, **(c)** Ni_2P and **(d)** $CoNi_3P$ samples.

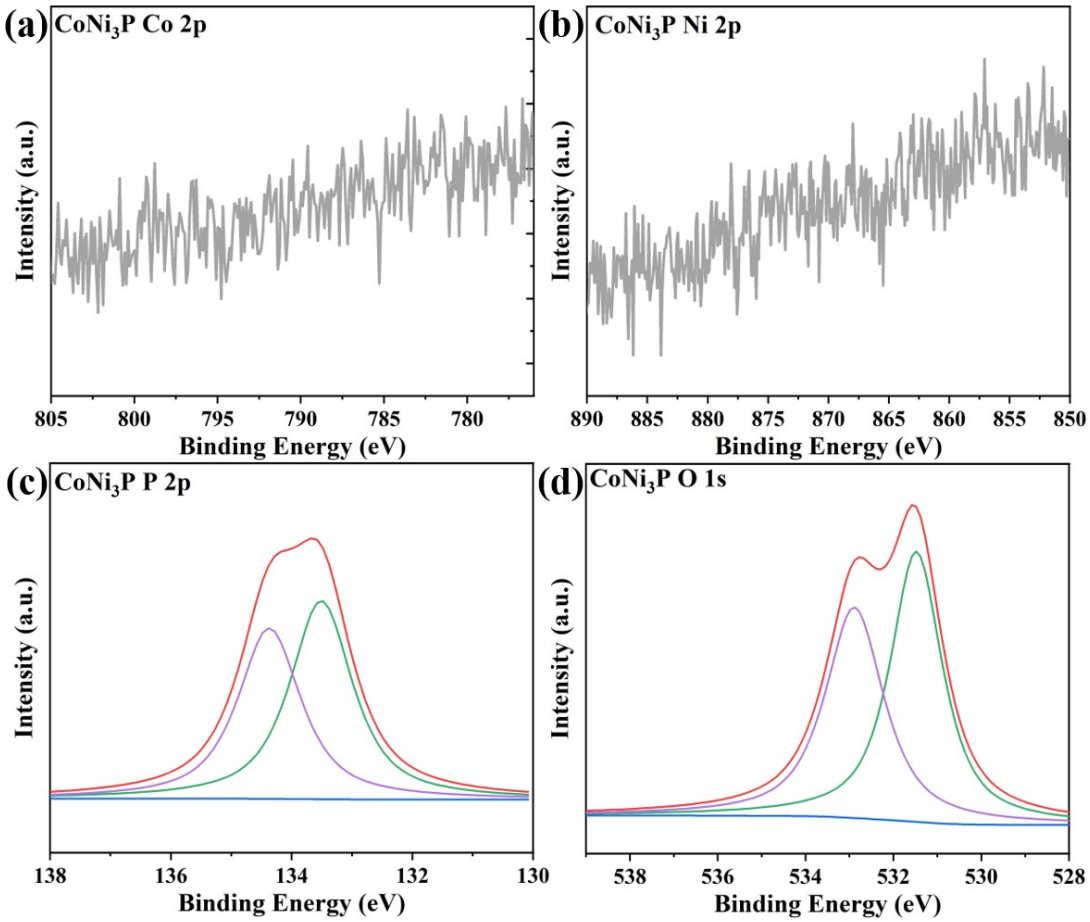

Figure S6. The High-resolution XPS spectra of **(a)** Co 2p, **(b)** Ni 2p, **(c)** P 2p and **(d)** O 1s of $CoNi_3P$ sample.

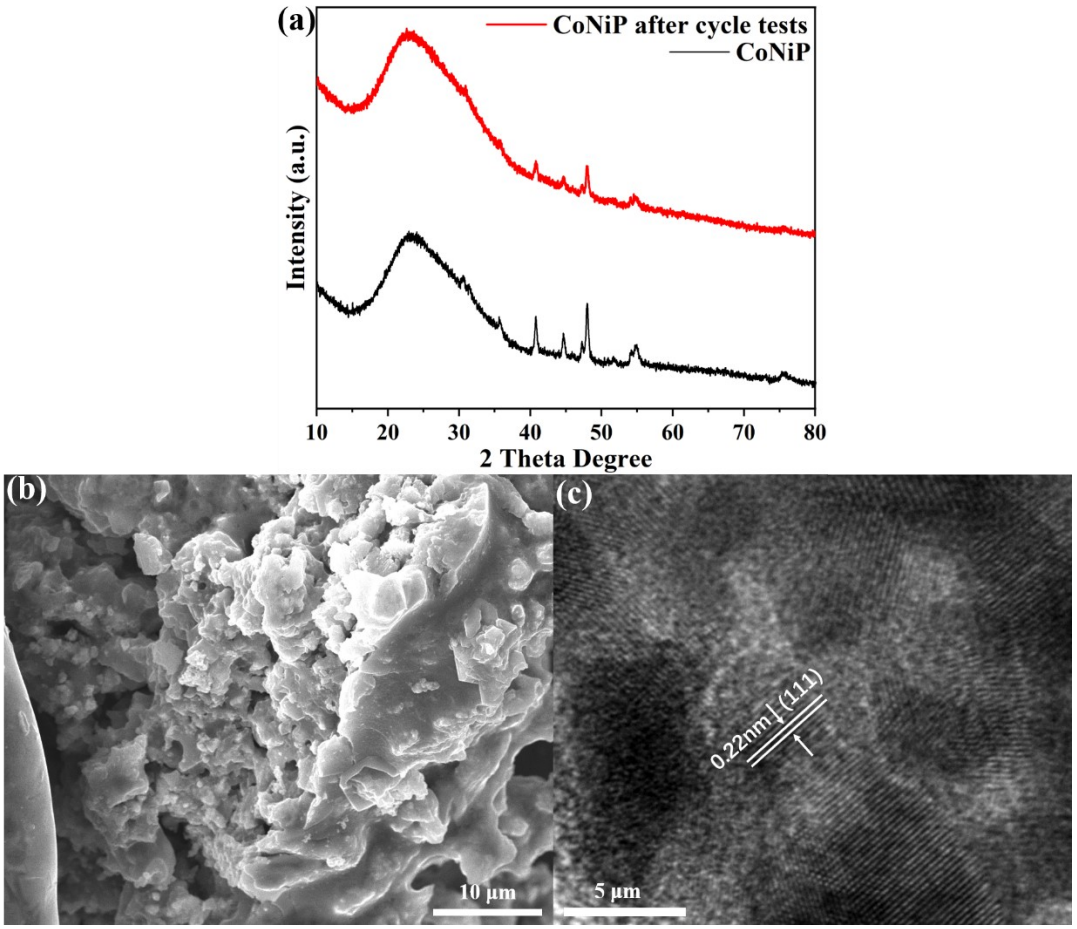

Figure S7. (a) The XRD pattern and **(b)** the SEM pattern of CoNiP sample after cycle stability test.

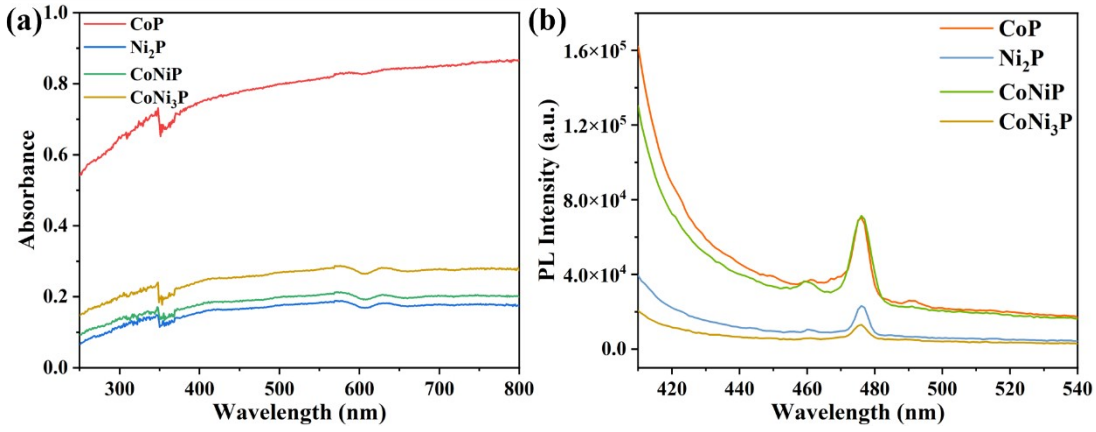

Figure S8. (a) The solid UV-Vis DRS and **(b)** the PL spectrum of CoP, Ni_2P, CoNiP and $CoNi_3P$ samples.

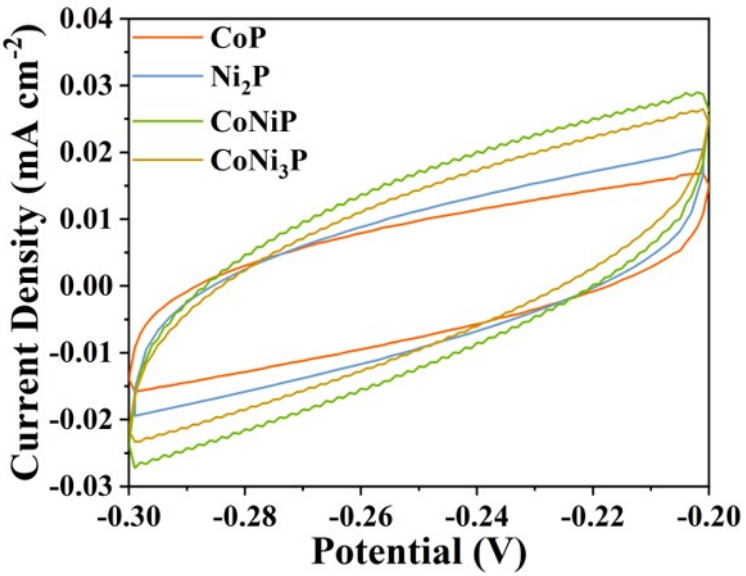

Figure S9. The specific capacitance performances (CV) of CoP, CoNiP, $CoNi_3P$ and Ni_2P samples.

Table S1. Comparison of recently reported earth-abundant metal catalysts for photocatalytic Eosin-Y sensitized H_2 evolution reaction.

Catalyst	**H_2 evolution rate (mmol g^{-1} h^{-1}) (Cal)**	**Reactant solution**	**Ref.**
CoNiP	**12.96**	**10% TEOA**	**This work**
10%-MCC/M–S	3.9	15% TEOA	R[4]
Co-NCNT-800	14.7	10% TEOA	R[5]
CoS	1.2	5% TEOA	R[6]
$Cu_{2-x}Se$	1.02	10.6% TEOA	R[7]
Ni@MOF-5	9.5	10% TEOA	R[8]
NiB/GO	6.5	10% TEOA	R[9]
$Ni(OH)_2/TiO_2$	1.6	5% TEOA	R[10]
Ni_2P-FG	2.26	10% TEOA	R[11]
Pt/C_3N_4	0.5	5% TEOA	R[12]
Pt/ZnO	3.9	10% TEOA	R[13]

rGO/MOF/Co-Mo-S	6.8	15% TEOA	R[14]
Sb doped SnO_2	0.25	10% TEOA	R[15]
Sn-doped ZnO/BiOCl	4.15	10% TEOA	R[16]
W-Co_3S_4	12.5	15% TEOA	R[17]
UiO-66-NH_2	2.76	10% TEOA	R[18]

References

1 G. Kresse and D. Joubert, *Phys. Rev. B*, 1999, **59**, 1758.

2 J. P. Perdew, K. Burke and M. Ernzerhof, *Phys. Rev. Lett.*, 1996, **77**, 3865–3868.

3 S. Grimme, J. Antony, S. Ehrlich and H. Krieg, *J. Chem. Phys.*, 2010, **132**, 154104.

4 T. Li, T. Yan and Z. Jin, *New J. Chem.*, 2021, **45**, 11905–11917.

5 X. Meng, Y. Dong, Q. Hu and Y. Ding, *ACS Sustain. Chem. Eng.*, 2019, **7**, 1753–1759.

6 M. Zheng, Y. Ding, L. Yu, X. Du and Y. Zhao, *Adv. Funct. Mater.*, 2017, **27**, 1605846.

7 H. Lim, I. Roh, J. Chung, J. Lee, J. W. Song and T. Yu, *J. Ind. Eng. Chem.*, 2023, **123**, 81–87.

8 W. Zhen, J. Ma and G. Lu, *Appl. Catal. B Environ.*, 2016, **190**, 12–25.

9 M. Q. Yang, J. Dan, S. J. Pennycook, X. Lu, H. Zhu, Q. H. Xu, H. J. Fan and G. W. Ho, *Mater. Horizons*, 2017, **4**, 885–894.

10 Z. Yan, X. Yu, Y. Zhang, H. Jia, Z. Sun and P. Du, *Appl. Catal. B Environ.*, 2014, **160**–**161**, 173–178.

11 S. H. Li, N. Zhang, X. Xie, R. Luque and Y. J. Xu, *Angew. Chem. Int. Ed.*, 2018, **57**, 13082–13085.

12 Y. Wang, J. Hong, W. Zhang and R. Xu, *Catal. Sci. Technol.*, 2013, **3**, 1703–1711.

13 D. Popugaeva, T. Tian and A. K. Ray, *Int. J. Hydrogen Energy*, 2020, **45**, 11097–11107.

14 D. Liu, Z. Jin and Y. Bi, *Catal. Sci. Technol.*, 2017, **7**, 4478–4488.

15 L. Yang, J. Huang, L. Shi, L. Cao, W. Zhou, K. Chang, X. Meng, G. Liu, Y. Jie and J. J. Ye, *Nano Energy*, 2017, **36**, 331–340.

16 Y. Guo, C. Qi, B. Lu and P. Li, *Int. J. Hydrogen Energy*, 2022, **47**, 228–241.

17 H. Wang and Z. Jin, *Sustain. Energy Fuels*, 2019, **3**, 173–183.

18 J. Shi, F. Chen, L. Hou, G. Li, Y. Li, X. Guan, H. Liu and L. Guo, *Appl. Catal. B Environ.*, 2021, **280**, 119385.